ARTICLE TYPE

Quantum interference and structure-dependent orbital-filling effects on the thermoelectric properties of quantum dot molecules

Chih-Chieh Chen,[ab] David M T Kuo,[∗c] and Yia-chung Chang[∗bd]

The quantum interference and orbital filling effects on the thermoelectric (TE) properties of quantum dot molecules with high figure of merit are illustrated via the full solution to the Hubbard-Andersono model in the Coulomb blockade regime. It is found that under certain condition in the triangular QD molecule (TQDM), destructive quantum interference (QI) can occur, which leads to vanishing small electrical conductance, while the Seebeck coefficient is modified dramatically. When TQDM is in the charge localization state due to QI, the Seebeck coefficient is seriously suppressed at low temperature, but highly enhanced at high temperature. Meanwhile, the behavior of Lorenz number reveals that it is easier to block charge transport via destructive QI than the electron heat transport at high temperatures. The maximum power factor (PF) in TQDM occurs at full-filling condition. Nevertheless, low-filling condition is preferred for getting maximum PF in serially coupled triple QDs in general. In double QDs, the maximum PF can be achieved either with orbital-depletion or orbital-filling as a result of electron-hole symmetry. Our theoretical work provides a useful guideline for advancing the nanoscale TE technology.

1 Introduction

To design solid-state coolers and power generators,[1–7] many efforts seek efficient thermoelectric (TE) materials with the figure of merit (ZT) larger than 3, which will lead to efficient TE conversion, making the TE device competitive with conventional air conditioners and power generators.[1,2] Furthermore, the energy harvesting by using TE materials is one of several advanced techniques considered for clean energies. The optimization of $ZT = S^2 G_e T/\kappa$ depends on the electrical conductance (G_e), Seebeck coefficient (S), and thermal conductance (κ). T is the equilibrium temperature. These physical quantities are usually related to one another. Mechanisms leading to the enhancement of power factor ($PF = S^2 G_e$) would also enhance the thermal conductance. Consequently, it is difficult to obtain ZT above one in conventional bulk materials.[1]

Recently, quantum dot superlattice (QDSL) nanowires

with impressive ZT values (larger than one) have been demonstrated experimentally.[8] The power factor and thermal conductance become independent thermoelectric variables under the condition $\kappa_e/\kappa_{ph} \ll 1$, where κ_e and κ_{ph} denote, respectively, the electron thermal conductance and phonon thermal conductance.[8] In the Coulomb blockade regime, electron transport process is seriously suppressed by the electron Coulomb interactions, causing κ_e and G_e to be reduced simultaneously.[9] On the other hand, under the condition $\kappa_e/\kappa_{ph} \ll 1$, one can increase the power factor (PF)[10–15] and decrease the phonon thermal conductance[16–21] simultaneously to optimize ZT. The ZT enhancement of QDSL mostly arises from changes induced by dimensional confinement in the electronic band structures as well as enhanced phonon scattering resulting from the scattering at nanowire surface and interfaces surrounding QDs.[1,2]

Although many theoretical efforts have investigated the PF enhancement of QDs[10–15] and molecule junctions[22–24], quantum interference (QI) and orbital filling effects on the PF optimization are still puzzling due to the difficulty to treat many body effect reliably in either QDSLs or molecules.[25] For example, in the triangular QD molecule (TQDM), there are 923 electron correlation functions appeared in the 4752 Green's functions need to be solved, when electron Coulomb interactions are turned

[a] Department of Physics, University of Illinois at Urbana-Champaign, Urbana, Illinois 61801, USA.
[b] Research Center for Applied Sciences, Academic Sinica, Taipei, 11529 Taiwan. E-mail: yiachang@gate.sinica.edu.tw
[c] Department of Electrical Engineering and Department of Physics, National Central University, Chungli, 320 Taiwan. E-mail: mtkuo@ee.ncu.edu.tw
[d] Department of Physics, National Cheng-Kung University, Tainan, 70101 Taiwan.

on, even though one just considers one energy level for each QD. As a consequence, a theoretical framework to treat adequately the many-body problem of a molecular junction remains elusive. QI is a remarkable effect, which influences the charge transport of QD array [6,8] and molecules [22–24] with multiple quantum paths. When the energy levels of QDSLs or molecules are below the Fermi energy of electrodes, the orbital filling effects can not be avoided for charge/heat transport. To reveal the many-body effects on the TE properties of QD junction system, we theoretically investigate QD molecules (QDMs), including double QD molecule (DQD)(see supplemental material), serially coupled triple QDs (SCTQD), and TQDM with a full many-body solution which takes into account all correlation functions resulting from electron Coulomb interactions in QDMs. Our results indicate that the effects of QI and structure-dependent orbital filling are quite significant in determining the behaviors of TE coefficients for junctions of coupled QDs.

2 Model

Here we consider nanoscale semiconductor QDs, in which the energy level separations are much larger than their on-site Coulomb interactions and thermal energies. Thus, only one energy level for each quantum dot needs to be considered. An extended Hubbard-Anderson model is employed to simulate a QDMs connected to electrodes (see the inset of Fig. 1(b)). The model is suitable in describing the electron transport in semiconductor quantum dot systems. [26,27] The Hamiltonian of the QDM junction is given by $H = H_0 + H_{QD}$:

$$
\begin{aligned}
H_0 &= \sum_{k,\sigma} \epsilon_k a_{k,\sigma}^\dagger a_{k,\sigma} + \sum_{k,\sigma} \epsilon_k b_{k,\sigma}^\dagger b_{k,\sigma} \\
&+ \sum_{k,\sigma} V_{k,L} d_{L,\sigma}^\dagger a_{k,\sigma} + \sum_{k,\sigma} V_{k,R} d_{R,\sigma}^\dagger b_{k,\sigma} + c.c
\end{aligned} \tag{1}
$$

where the first two terms describe the free electron gas of left and right electrodes. $a_{k,\sigma}^\dagger$ ($b_{k,\sigma}^\dagger$) creates an electron of momentum k and spin σ with energy ϵ_k in the left (right) electrode. $V_{k,\ell}$ ($\ell = L, R$) describes the coupling between the electrodes and the left (right) QD. $d_{\ell,\sigma}^\dagger$ ($d_{\ell,\sigma}$) creates (destroys) an electron in the ℓ-th dot.

$$
\begin{aligned}
H_{QD} &= \sum_{\ell,\sigma} E_\ell n_{\ell,\sigma} + \sum_\ell U_\ell n_{\ell,\sigma} n_{\ell,\bar\sigma} \\
&+ \frac{1}{2} \sum_{\ell,j,\sigma,\sigma'} U_{\ell,j} n_{\ell,\sigma} n_{j,\sigma'} + \sum_{\ell,j,\sigma} t_{\ell,j} d_{\ell,\sigma}^\dagger d_{j,\sigma},
\end{aligned} \tag{2}
$$

where E_ℓ is the spin-independent QD energy level, and $n_{\ell,\sigma} = d_{\ell,\sigma}^\dagger d_{\ell,\sigma}$. Notations U_ℓ and $U_{\ell,j}$ describe the intradot and interdot Coulomb interactions, respectively. $t_{\ell,j}$ describes the electron interdot hopping. Noting that the interdot Coulomb interactions as well as intradot Coulomb interactions play a significant role on the charge transport for semiconductor QDs [9] and molecular structures. [22–24]

Using the Keldysh-Green's function technique, [26,27] the charge and heat currents from reservoir α to the QDM junction are calculated according to the Meir-Wingreen formula

$$
\begin{aligned}
J_\alpha &= \frac{ie}{h} \sum_{j\sigma} \int d\epsilon \Gamma_j^\alpha(\epsilon) [G_{j\sigma}^<(\epsilon) + f_\alpha(\epsilon)(G_{j\sigma}^r(\epsilon) \\
&- G_{j\sigma}^a(\epsilon))] \tag{3} \\
Q_\alpha &= \frac{i}{h} \sum_{j\sigma} \int d\epsilon (\epsilon - \mu_\alpha) \Gamma_j^\alpha(\epsilon) [G_{j\sigma}^<(\epsilon) + f_\alpha(\epsilon) \\
&(G_{j\sigma}^r(\epsilon) - G_{j\sigma}^a(\epsilon))], \tag{4}
\end{aligned}
$$

Notation $\Gamma_\ell^\alpha = \sum_k |V_{k,\alpha,\ell}|^2 \delta(\epsilon - \epsilon_k)$ is the tunneling rate between the α-th reservoir and the ℓ-th QD. $f_\alpha(\epsilon) = 1/\{\exp[(\epsilon - \mu_\alpha)/k_B T_\alpha] + 1\}$ denotes the Fermi distribution function for the α-th electrode, where μ_α and T_α are the chemical potential and the temperature of the α electrode. $\mu_L - \mu_R = \Delta V$ and $T_L - T_R = \Delta T$. e, h, and k_B denote the electron charge, the Planck's constant, and the Boltzmann constant, respectively. $G_{j\sigma}^<(\epsilon)$, $G_{j\sigma}^r(\epsilon)$, and $G_{j\sigma}^a(\epsilon)$ are the frequency domain representations of the one-particle lessor, retarded, and advanced Green's functions $G_{j\sigma}^<(t,t') = i\langle d_{j,\sigma}^\dagger(t') d_{j,\sigma}(t)\rangle$, $G_{j\sigma}^r(t,t') = -i\theta(t - t')\langle\{d_{j,\sigma}(t), d_{j,\sigma}^\dagger(t')\}\rangle$, and $G_{j\sigma}^a(t,t') = i\theta(t' - t)\langle\{d_{j,\sigma}(t), d_{j,\sigma}^\dagger(t')\}\rangle$, respectively. These one-particle Green's functions are related recursively to other Green's functions and density-density correlators via the few-body equation of motion, [25] which we solve via an iterative numerical procedure to obtain all n-particle Green's functions and correlators for the QDM. The coupling between electrons in the leads and electrons in QDM is included in the self-energy term, Γ_ℓ^α. Because of this approximation, our procedure is valid only in the Coulomb blockade regime, but not the Kondo regime. [28]

Thermoelectric coefficients in the linear response

regime are

$$G_e = (\frac{\delta J_\alpha}{\delta \Delta V})_{\Delta T=0} \tag{5}$$

$$S = -(\frac{\delta J_\alpha}{\delta \Delta T})_{\Delta V=0}/(\frac{\delta J_\alpha}{\delta \Delta V})_{\Delta T=0} \tag{6}$$

$$\kappa_e = (\frac{\delta Q_\alpha}{\delta \Delta T})_{\Delta V=0} + (\frac{\delta Q_\alpha}{\delta \Delta V})_{\Delta T=0}S \tag{7}$$

$$= (\frac{\delta Q_\alpha}{\delta \Delta T})_{\Delta V=0} - S^2 G_e T$$

where

$$(\frac{\delta J_\alpha}{\delta \Delta V})_{\Delta T=0} = \frac{ie}{h}\sum_{j\sigma}\int d\epsilon \Gamma_j^\alpha(\epsilon) \times \tag{8}$$

$$[\frac{\delta G_{j\sigma}^<(\epsilon)}{\delta f_\alpha(\epsilon)} + (G_{j\sigma}^r(\epsilon) - G_{j\sigma}^a(\epsilon))]\frac{\delta f_\alpha(\epsilon)}{\delta \Delta V},$$

$$(\frac{\delta J_\alpha}{\delta \Delta T})_{\Delta V=0} = \frac{ie}{h}\sum_{j\sigma}\int d\epsilon \Gamma_j^\alpha(\epsilon) \times \tag{9}$$

$$[\frac{\delta G_{j\sigma}^<(\epsilon)}{\delta f_\alpha(\epsilon)} + (G_{j\sigma}^r(\epsilon) - G_{j\sigma}^a(\epsilon))]\frac{\delta f_\alpha(\epsilon)}{\delta \Delta T},$$

$$(\frac{\delta Q_\alpha}{\delta \Delta T})_{\Delta V=0} = \frac{i}{h}\sum_{j\sigma}\int d\epsilon \Gamma_j^\alpha(\epsilon)(\epsilon - E_F) \times \tag{10}$$

$$[\frac{\delta G_{j\sigma}^<(\epsilon)}{\delta f_\alpha(\epsilon)} + (G_{j\sigma}^r(\epsilon) - G_{j\sigma}^a(\epsilon))]\frac{\delta f_\alpha(\epsilon)}{\delta \Delta T},$$

$$(\frac{\delta Q_\alpha}{\delta \Delta V})_{\Delta T=0} = \frac{i}{h}\sum_{j\sigma}\int d\epsilon \Gamma_j^\alpha(\epsilon)(\epsilon - E_F) \times \tag{11}$$

$$[\frac{\delta G_{j\sigma}^<(\epsilon)}{\delta f_\alpha(\epsilon)} + (G_{j\sigma}^r(\epsilon) - G_{j\sigma}^a(\epsilon))]\frac{\delta f_\alpha(\epsilon)}{\delta \Delta V}.$$

The quantity $\frac{\delta G_{j\sigma}^<(\epsilon)}{\delta f_\alpha(\epsilon)}$ is obtained by solving the variation of the equation of motion with respect to the change in Fermi-Dirac distribution, $f_\alpha(\epsilon)$. Here we have assumed the variation of the correlation functions with respect to $\delta f_\alpha(\epsilon)$ is of the second order. Note that we have to take $\Delta V \to 0$ for the calculations of $(\frac{\delta J_\alpha}{\delta \Delta V})_{\Delta T=0}$ and $(\frac{\delta Q_\alpha}{\delta \Delta V})_{\Delta T=0}$. Meanwhile we taken $\Delta T \to 0$ for Eqs. (9) and (10). E_F is the Fermi energy of electrodes. There is a Joule heating term $\Delta V \times J_\alpha$ arising from Eq. (4) which can be ignored in the linear response regime.

It is a challenge to prove that whether the Eqs. (3) and (4) can be expressed in terms of transmission coefficient (or Landauer's expression) when one takes into account all Green's functions and correlation functions fully. To gain deeper insight into the electron correlation effect, we adopt the approximation procedure of Kuo and Chang[9] and obtain $G_e = e^2 \mathcal{L}_0$, $S = -\mathcal{L}_1/(eT\mathcal{L}_0)$ and $\kappa_e = \frac{1}{T}(\mathcal{L}_2 - \mathcal{L}_1^2/\mathcal{L}_0)$, which can be calculated by a closed form expression for the transmission coefficient. $\mathcal{L}_n$ is given by

$$\mathcal{L}_n = \frac{2}{h}\int d\epsilon \mathcal{T}_{LR}(\epsilon)(\epsilon - E_F)^n \frac{\partial f(\epsilon)}{\partial E_F}, \tag{12}$$

where $\mathcal{T}_{LR}(\epsilon)$ is the transmission coefficient. $f(\epsilon) = 1/(exp^{(\epsilon-E_F)/k_B T} + 1)$. The thermoelectric coefficients determined by Eq. (12) are employed to compare with results of Eqs. (5)-(7). Because the condition $\kappa_e/\kappa_{ph} \ll 1$ is readily satisfied in the Coulomb blockade regime,[9] the optimization of ZT can be improved by finding the best power factor ($PF = S^2 G_e$).

3 Results and discussion

3.1 Effect of destructive QI

First, we consider a TQDM with electron hopping strengths $t_{LC} = t_{CR} = t_c \neq t_{LR}$. Figure 1 shows the electrical conductance and Seebeck coefficient as functions of the energy level of central QD ($\Delta_C = E_C - E_F$) for various coupling strengths, t_{LR} at $k_B T = 1\Gamma_0$. In the small Δ_C regime ($\Delta_C \leq 10\Gamma_0$) G_e is found to be insensitive to t_{LR}, because the charge transport is dominated by the near-resonant tunneling process through levels at $E_F + \sqrt{2}t_c$, E_F and $E_F - \sqrt{2}t_c$. On the other hand, G_e changes significantly with the variation of t_{LR} in the regime of $\Delta_C/\Gamma_0 \geq 10$. For $t_{LR} = 0.1\Gamma_0$, G_e is vanishingly small at $\Delta_{C4} = 90\Gamma_0$. The minimum of G_e occurs at lower Δ_C if t_{LR} is increased. For example, the minimum of G_e occurs at $\Delta_{C3} = 45\Gamma_0$, $\Delta_{C2} = 30\Gamma_0$, and $\Delta_{C1} = 22.5\Gamma_0$ for $t_{LR} = 0.2\Gamma_0$, $t_{LR} = 0.3\Gamma_0$ and $t_{LR} = 0.4\Gamma_0$, respectively. This behavior is caused by the quantum interference (QI) between two paths. This direct coupling (t_{LR}) between the outer QDs provides one path. The long distance coherent tunneling (LDCT)[25] mediated by the central QD provides another path, which leads to an effective electron hopping strength $t_{eff} = -t_{LC}t_{CR}/\Delta_C$ between the outer QDs. Such an effective coupling between outer dots can be used to manipulate the spin entanglement between dots separated by a long distance.[29–31] We note that the vanishingly small G_e occurs when the condition of $|t_{eff}| = t_{LR}$ is met.

To depict the behavior of Fig. 1(a), we also calculate G_e by using the approximate expression, $\mathcal{T}_{LR}^1(\epsilon)$ for transmission coefficient as given below.

$$\mathcal{T}_{LR}^1(\epsilon) \tag{13}$$

$$= \frac{4\Gamma_L \Gamma_R P_1 F_{QI}}{|\mu_1\mu_2\mu_3 - t_{CR}^2\mu_1 - t_{LC}^2\mu_3 - t_{LR}^2\mu_2 - 2t_{LR}t_{LC}t_{CR}|^2},$$

where $\mu_1 = \epsilon - E_L + i\Gamma_L$, $\mu_2 = \epsilon - E_C$ and $\mu_3 = \epsilon - E_R + i\Gamma_R$. $P_1 = (1 - N_{L,\bar{\sigma}})(1 - N_{C,\bar{\sigma}} - N_{C,\sigma} + c_C)(1 - N_{R,\bar{\sigma}} - N_{R,\sigma} + c_R)$ denotes the probability weight of electron transport through TTQD in an empty state, which is
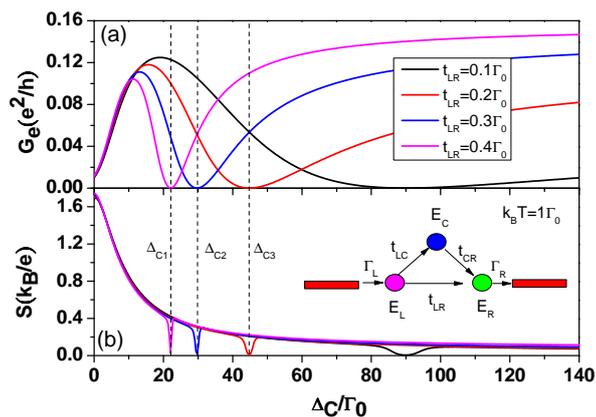
Fig. 1 (a) Electrical conductance (G_e) and (b) Seebeck coefficient (S) of TQDM as a function of central QD energy ($\Delta_C = E_C - E_F$) for different t_{LR} strengths at $E_L = E_R = E_F$, $t_{LC} = t_{CR} = t_c = 3\Gamma_0$ and $k_B T = 1\Gamma_0$. We assume $U_{LC} = U_{CR} = 30\Gamma_0$, $U_{LR} = 10\Gamma_0$, $U_\ell = U_0 = 100\Gamma_0$ and $\Gamma_L = \Gamma_R = \Gamma = 0.3\Gamma_0$.

determined by the one particle occupation number ($N_{\ell,\bar\sigma}$) and on-site two particle correlation functions (c_ℓ) resulting from electron Coulomb interactions. P_1 equals to one in the absence of electron Coulomb interactions. The numerator $F_{QI} = (t_{LC} t_{CR} + t_{LR}\mu_2)^2$ causes the QI effect. The first term and the second term of F_{QI} describe, respectively, the "L-C-R" path through the central QD and the "L-R" path for direct hopping between the outer QDs. Due to $t_{LC} = t_{CR} = t_c \neq t_{LR}$, there are three poles in the denominator of Eq. (13). If we take $\Gamma = 0$, the poles occur at

$$\epsilon_\pm = \frac{E_C + E_0 + t_{LR}}{2} \pm \frac{1}{2}\sqrt{(E_C - E_0 - t_{LR})^2 + 8t_C^2}$$
$$\epsilon_0 = E_0 - t_{LR}. \tag{14}$$

Here, $E_0 = E_L = E_R = E_F$ in Eq. (14). For higher symmetry TQDM ($t_{LR} = t_{LC} = t_{CR} = t_c$ and $E_\ell = E_0$), we have $\epsilon_+ = E_0 + 2t_c$, $\epsilon_- = E_0 - t_c$ and $\epsilon_0 = E_0 - t_c$.

Once $\Delta_C = E_C - E_F \gg 2t_c$, the lowest energy level is given by $\epsilon_0 = E_0 - t_{LR}$. Keeping only the resonant channel at ϵ_0, we obtain

$$G_e = \frac{2e^2}{h}\frac{\Gamma\pi}{4k_B T}\frac{(t_{eff} + t_{LR})^2}{(t_{LR} + t_{eff})^2 + (\Gamma/2)^2}\frac{P_1}{cosh^2(\frac{t_{LR}}{2k_B T})}, \tag{15}$$

where $t_{eff} = -t_c^2/\Delta_C$. This expression can well explain the destructive QI behavior shown in Fig. 1(a). According to Eq. (13), the QI observed in Fig. 1(a) will disappear as $t_{LR} = 0$ (the case of SCTQD). In Sánchez *et al.*[32] it was proposed that destructive QI of two superexchange

trajectories can also occur in SCTQD. Note that such an effect is easily masked by the background current at finite temperatures. Thus, it is not as robust as the QI effect described here. Using Eq. (12) and considering the ϵ_0 pole of Eq. (14), we can show that $S = t_{LR}/T$ is positive and independent on Δ_C. However, $S = t_{LR}/T$ can not describe the behavior of S shown in Fig. 1(b) (obtained by the full calculation), which is a function of Δ_C. This implies that the resonant channels involving E_C can not be ignored for calculating S in the regime of $t_{eff}/t_{LR} > 1$. The positive sign of S indicates that the hole diffusion dominates over electron diffusion at low temperature ($k_B T = 1\Gamma_0$). Here holes are defined as missing electrons in states below E_F. The results of Fig. 1(a) show that the Seebeck coefficient is seriously suppressed under the destructive QI effect. Such a behavior is quite different from the general behavior of Seebeck coefficient observed in QD junction systems.[10–15] (See results of Figs. 5-7 and note that the minimum of S occurs at the maximum of G_e.

To further clarify the above destructive QI behavior, we plot the electrical conductance and Seebeck coefficient at various temperatures for $t_{LR} = 0.3\Gamma_0$ in Fig. 2. It shows that G_e is suppressed with increasing temperature. Meanwhile, the destructive QI effect on G_e is very robust with respect to temperature variation when $k_B T$ is tuned up to $5\Gamma_0$. The results of Fig. 2(a) imply that a single-electron QI transistor is achievable even at room temperature.[33] The change of sign for S from positive to negative indicates that the resonant channels above E_F become important with increasing temperature with electron contribution dominating over hole contribution. In particular, we noticed a large enhancement of the negative S peak at Δ_{QI} (the value of Δ_C where QI occurs) as temperature increases. Namely, the Seebeck coefficient changes sign and enhances with increasing temperature. We also noticed that peak value of $|S|$ reaches a maximum near $k_B T = 4\Gamma_0$ and decreases afterwards.

To reveal the importance of electron correlation effects and understand the interesting behavior of S in Fig. 2(b), we recalculate the results of Fig. 2 with the procedure given in Ref. 9. There are 32 configurations in the transmission coefficient of Eq. (12) for electrons with spin $\bar\sigma$ in the electrodes. The expression of Eq. (13) is for an empty TQDM. The curves in Fig. 3 have one-to-one correspondence to those of Fig. 2. We found significant differences between Fig. 2(a) and Fig. 3(a), when Δ_C is smaller than 20 Γ_0. This implies that the electron correlation effects become important when E_C closes to E_F. In particular, two-particle interdot correlation functions. However, both approaches give similar QI effect with the same value for Δ_{QI}. This is because QI is mainly caused by
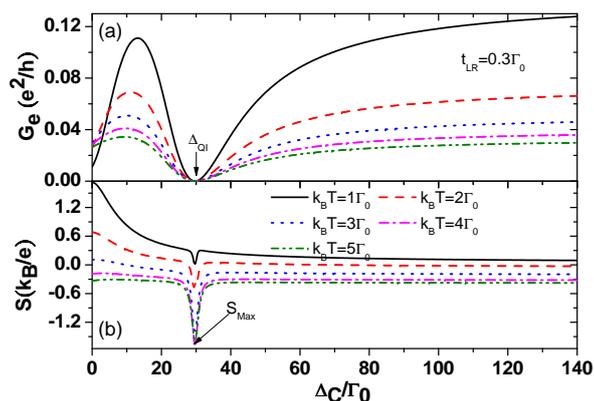
Fig. 2 (a) Electrical conductance (G_e) and (b) Seebeck coefficient (S) of TQDM as a function of central QD energy ($\Delta_C = E_C - E_F$) at $t_{LR} = 0.3\Gamma_0$ for different temperatures. Other physical parameters are the same as those of Fig. 1.

Fig. 3 The curves of Fig. 3 are one to one corresponding to those of Fig. 2. The calculation of Fig. 3 only considers the single particle occupation numbers and on-site two particle correlation functions.

the single-particle transport process. Fig. 3(b) also shows enhancement of $|S|$ at Δ_{QI} with increasing temperature, but the degree of enhancement is overestimated compared with the full calculation. The temperature dependence of S_{max} (at Δ_{QI}) is plotted in the inset of Fig. 3(b). It is seen that S_{max} obeys the simple relation $S \approx -\frac{U_{LR}}{T}$ when $k_B T > 2\Gamma_0$. One can show that the next important contribution to S is from the resonant channel near $\epsilon = E_0 + U_{LR} - t_{LR}$, but not from ϵ_+ given by Eq. (14). Note that the contribution of this resonant channel to G_e is small compared to the ϵ_0 channel. To demonstrate the effect of electron Coulomb interactions, we plot the curve with red triangle marks for $U_\ell = U_{\ell,j} = 0$ at $k_B T = 2\Gamma_0$. Now, $S_{max} = t_{LR}/T$ becomes very small in the absence of electron Coulomb interactions. This proves that the enhancement of $|S_{max}|$ results from the resonant channels involving electron Coulomb interactions. This also explains the enhancement of $|S_{max}|$ shown in Fig. 2(b).

According to the results of Figs. (1) and (2), the destructive QI effect can blockade the charge transport. Next, we clarify how QI influences electron heat transport. Fig. 4 shows the electron thermal conductance (κ_e) and Lorenz number ($L_z = \kappa_e/(G_e T)$) as functions of Δ_C. The physical parameters adopted in the calculation are the same as those for Fig. 2. Like G_e, the electron heat transport can be modulated by tuning the central QD energy level. We see that the electron thermal conductance is also vanishingly small at $\Delta_{QI} = 30\Gamma_0$ due to the destructive QI. There is the Wiedemann-Franz law in metals to link two physical quantities (G_e and κ_e). Here, we recheck the Wiedemann-Franz law by

calculating the Lorenz number in Fig. 4(b). A highly temperature-dependent behavior of L_z occurs at Δ_{QI}. The fact that L_z larger than one indicates that it is easier to block charge transport via destructive QI than the electron heat transport. In metals the Lorenz number is a universal constant $L_z = \frac{\pi^2}{3}(k_B/e)^2$, which is independent of T. Our results obviously violet the Wiedemann-Franz law near $\Delta_C = \Delta_{QI}$ for all temperatures. The violation of Wiedemann-Franz law is a typical phenomenon for nanostructures with discrete energy levels.[3] The QI effects on the TE properties are illustrated by using QDMs with N=3 as an example. The unsymmetrical features of $t_{LC} = t_{CR} \neq t_{LR}$, $U_{LC} = U_{CR} \neq U_{LR}$, and $E_L = E_R \neq E_C$ considered in TQDM can be used to reveal the effects of QD size fluctuation and nonuniform interdot separation on the charge transport of QDSL system.[6,8]

3.2 Orbital filling effects

Many theoretical studies have used the Hartree-Fock approximation (HFA) to predict the TE coefficients of realistic molecules with orbital below the E_F of electrodes.[22–24] Such a mean-field approach does not take full account of the electron correlation effects. Therefore, the predicted G_e, S and PF can not reveal the realistic TE properties of molecule junction systems in the Coulomb blockade regime. To reveal the orbital charge-filling (orbital below E_F) effects on the thermoelectric properties of TTQD, we plot the total occupation number ($N = \sum_\sigma (N_{L,\sigma} + N_{c,\sigma} + N_{R,\sigma})$), G_e and S as functions of gate voltage V_g ($E_\ell = E_F + 30\Gamma_0 - eV_g$) at $\Gamma = 0.3\Gamma_0$,
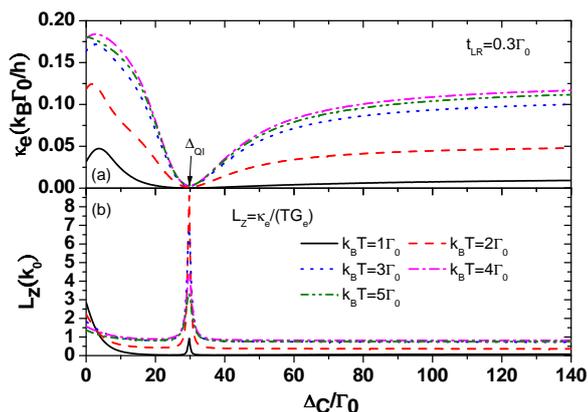
Fig. 4 (a) Electron thermal conductance (κ_e), and (b) Lorenz number($\kappa_e/(G_e T)$) as a function of central QD energy for different temperatures. The curves of Fig. 4 correspond to those of Fig. 2. $k_0 = k_B^2/e^2$.

$t_{\ell,j} = 3\Gamma_0$ and $U_{\ell,j} = 30\Gamma_0$ for various temperatures in Fig. 5. Here, the QD energy levels are placed at $30\Gamma_0$ above E_F when $eV_g = 0$. The average total occupation number (N) display an staircase behavior with six plateaus. The step edges are broadened as temperature increases. The height of each staircase is equal to one. The onsets of these plateaus are roughly determined by $U_{\ell,j}$ and U_ℓ. Therefore, the electron number of TQDM is tuned from one to six with increasing gate voltage. The spectrum of G_e exhibits a Coulomb oscillation behavior with respect to gate voltage. Six main peaks of G_e labeled by ϵ_n correspond to the particle-addition energy of TQDM with different many-body states. For $k_B T = 1\Gamma_0$, there are several insulating states (with vanishingly small G_e). Such insulating states are not due to the QI effect, but the Coulomb blockade effect. The regime of vanishingly small G_e is related to a very small transmission coefficient resulting from the absence of resonant levels near E_F. The insulating state of a single benzene molecule calculated by the HFA method was suggested from the destructive QI effect. [22–24] The suggestions from Refs [22-24] unclear due to deficiency of mean field theory in the Coulomb blockade regime. [22] Although the behavior of G_e with respect to $k_B T$ is a typical behavior that the magnitude of G_e peak is suppressed with increasing temperature, meanwhile the width of each peak becomes broadened, we find a more dramatic reduction of ϵ_6 peak when $k_B T$ is tuned from $1\Gamma_0$ to $2\Gamma_0$. In addition, the peak position is shifted with increasing temperature. Several secondary peaks resulting from excite states around these main peaks are washed out by in-

creasing temperature. The separation between ϵ_3 and ϵ_4 is the so called "Coulomb gap" (these two peaks are separated by the intradot Coulomb interaction U_ℓ). [25] Using the middle Coulomb gap as a reference point, the G_e spectrum does not maintain the mirror symmetry. This is different from that of DQDs.
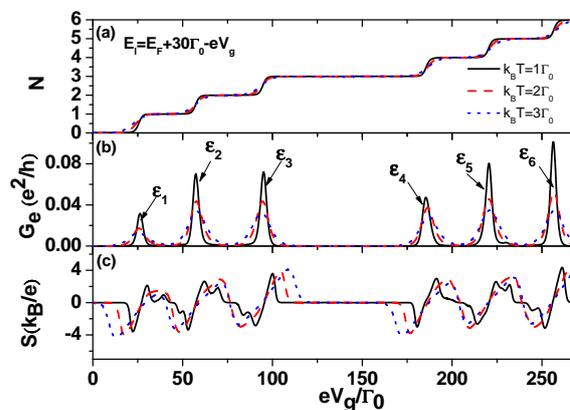
Fig. 5 (a) Total occupation number, (b) electrical conductance (G_e), and (c) Seebeck coefficient (S) as a function of QD energy ($E_\ell = E_F + 30\Gamma_0 - eV_g$) at $t_{\ell,j} = 3\Gamma_0$ and $U_{\ell,j} = 30\Gamma_0$ for different temperatures. Other physical parameters are the same as those of Fig. 1.

The Seebeck coefficient shown in Fig. 5(c) also shows an oscillatory behaviors with respect to gate voltage. When QD energy levels are above E_F the Seebeck coefficients are negative, which indicates that electrons dominate the diffusion process of thermoelectric properties. When QD energy levels near E_F, S almost vanishes due to the electron-hole balance. The positive S indicates that holes through resonant level below E_F become majority carriers. Such bipolar effects is the interplay between holes and electrons. When the resonant levels corresponding to the two-electron and three-electron states of TQDM (ϵ_2 and ϵ_3) are near E_F, once again the Seebeck coefficients become very small. We note that when G_e reaches the maximum, the Seebeck coefficient (S) reaches zero. This is different from that of Fig. 2. The Seebeck coefficient near the onsets of plateaus for $N = 1, 3, 4$, and 6 are highly enhanced with increasing temperature. Like the G_e spectrum, the Seebeck coefficient does not exhibit a mirror symmetry. We find prominent secondary oscillatory structures of S (clearly noticeable at $k_B T = 1\Gamma_0$), which arise from the secondary resonant levels around the main peaks of G_e. Compared to the spectrum of G_e at low temperature, the spectrum of S can clearly resolve the structures arising from the excited states (secondary

resonances) of TQDM. Consequently, the measurement of S is a powerful means to reveal various configurations of TQDM arising from the many-body effect. Unlike the case of metallic QDs,[34] the spectrum of S does not show the periodically oscillating structure with respect to the gate voltage due to $U_\ell \neq U_{\ell,j}$ and electron correlation effects, indicating that the interdot Coulomb interactions and intradot Coulomb interactions both play significant role in the electron transport.

To examine the interdot Coulomb interaction effects, Figure 6 shows (a) the electrical conductance, (b) Seebeck coefficient and (c) power factor as functions of V_g for three different values of $U_{\ell,j}$ at $k_B T = 1\Gamma_0$. Other physical parameters are the same as those of Fig. 5. From the results of G_e, we find that the interdot Coulomb interactions not only influence the peak positions, but also change the magnitude of each peak. For $U_{\ell,j} = 0$, the G_e spectrum shows only four peaks (see blue dashed line). The first two peaks (separated by $3t_c$) correspond to the resonant levels $\epsilon_{BD} = E_0 - t_c$ (bonding state) and $\epsilon_{AB} = E_0 + 2t_c$ (antibonding state). It is noted that the first G_e peak at ϵ_{BD} is significantly reduced and the second peak at ϵ_{AB} is totally suppressed when $U_{\ell,j}$ becomes finite.
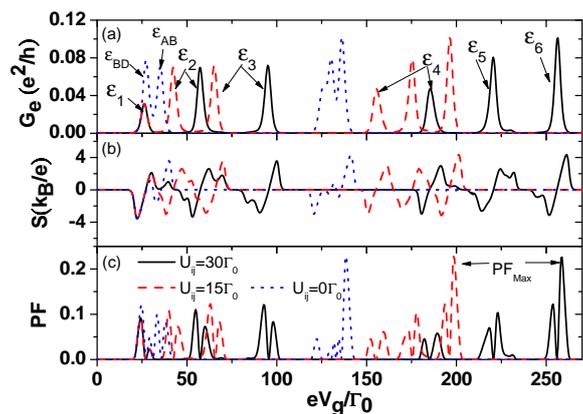
Fig. 6 (a) Electrical conductance (G_e), (b) Seebeck coefficient (S) and (c) power factor as a function of QD energy ($E_\ell = E_F + 30\Gamma_0 - eV_g$) at $t_{\ell,j} = t_c = 3\Gamma_0$ and $k_B T = 1\Gamma_0$ for different interdot Coulomb interactions. Other physical parameters are the same as those of Fig. 5.

The peak structures of the G_e spectrum for $U_{\ell,j} = 15\Gamma_0$ is quite similar to that for $U_{\ell,j} = 30\Gamma_0$, except the spacings between peaks are different, which leads to very different behavior in the Seebeck coefficient. Previous theoretical works predicted the thermal power (or Seebeck coefficient) spectra without considering interdot Coulomb

interactions.[15] This is inadequate for studying semiconductor QD molecules with nanoscale separation between QDs. Our calculations indicate that to achieve large maximum power factor (PF_{max}) in TQDM with homogenous QD energy levels and electron hopping strengths, the full-filling condition (with six-electron state) is preferred. This is due to the fact that three resonant channels associated states localized at dot L, C, and R (with energies at $E_L + U_0 + 2U_{LC} + 2U_{LR}$, $E_C + U_0 + 2U_{LC} + 2U_{CR}$, and $E_R + U_0 + 2U_{LR} + 2U_{CR}$, respectively) are all aligned. It is interesting to see what would happen in other QDM structures when the resonant conditions are changed.

Figure 7 shows G_e, S and PF of SCTQD as functions of V_g at different T. For simplicity, we adopt $t_{LR} = 0$ and $U_{LR} = 0$, since they are typically much smaller than the corresponding parameters related to the central dot. The G_e spectrum in Fig. 7 does not show the mirror symmetry as a result of the inhomogeneous interdot Coulomb interactions ($U_{LC} = U_{CR} \neq U_{LR}$). The peaks labeled ϵ_N ($N = 1, \cdots, 6$) correspond to the transitions where the total particle numbers in the SCTQD changes from $N-1$ to N with ϵ_1, ϵ_2, and ϵ_4 being more prominent. The ϵ_1 peak comes from electrons tunneling through the empty SCTQD via the resonant level $\epsilon_1 = E_0 - \sqrt{2}t_c$. The ϵ_2 peak ($\epsilon_2 = E_0 + \sqrt{2}t_c + U_{LR}$) corresponds to charge transport in the presence of another electron localized in one of the two outer dots. (Here we have chosen $U_{LR} = 0$) This is verified by examining $N_{C,\sigma}$, which is negligible until eV_g is near ϵ_3. $\epsilon_4 = E_0 + U_0 + U_{LC}(U_{CR})$ corresponds to the injection of an electron into the left (right) dot of SCTQD with all three dots each filled with one electrons, while $\epsilon_5 = E_0 + U_0 + U_{LC}(U_{CR}) + 2t_{eff}$ corresponds to the addition of another electron in either left or right dot to the configuration associated with ϵ_4, where $t_{eff} = t_{LC}t_{CR}/(E_F - (E_C + 2U_{LC} + 2U_{CR})) = 0.9\Gamma_0$ is the effective hopping strength mediated by the center dot. Therefore, the splitting between ϵ_4 and ϵ_5 can be observed by increasing $t_{\ell,j}$.

The Seebeck coefficient spectrum can reveal fine structures not resolved in the G_e spectrum. For example, the ϵ_3 and ϵ_6 peaks are hardly noticeable in G_e but clearly observable in S. The peak at $\epsilon_3 = E_0 + U_{LC} + U_{CR}$ is caused by the charging of the center dot with two outer dots each filled with one electron and ϵ_6 describes the charging of SCTQD with a second electron into the center QD with two outer dots each filled with two electrons. In strong contrast to TQDM, both G_e and PF of SCTQD are very small at the maximum filling condition ($N = 6$), which occurs at $eV_g = 250\Gamma_0$ where $E_C + U_0 + 2U_{LC} + 2U_{CR}$ is aligned with E_F. This is because the three resonant channels associated states localized at dot L, C, and R (with energies at $E_L + U_0 + 2U_{LC} + 2U_{LR}$, $E_C + U_0 +$
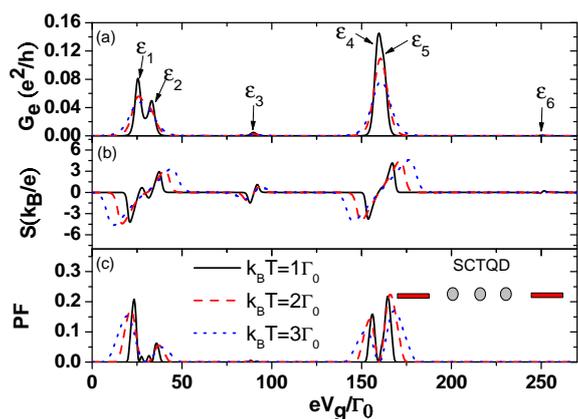
Fig. 7 Electrical conductance (G_e), Seebeck coefficient (S) and power factor of SCTQD as functions of QD energy ($E_\ell = E_F + 30\Gamma_0 - eV_g$) for different temperatures. $U_{LR} = 0$ and $t_{LR} = 0$. Other physical parameters are the same as those of Fig. 5.

$2U_{LC} + 2U_{CR}$, and $E_R + U_0 + 2U_{LR} + 2U_{CR}$, respectively) are misaligned, since $U_{LR} = 0$ (or $U_{LR} \ll U_{CR}$ in general). Consequently, charge transport is seriously suppressed for QD molecule with orbital-filling condition, which is expected to be a general feature in serially coupled QDMs with more dots. For the present SCTQD, the maximum PF occurs at the combined ϵ_4 and ϵ_5 peak as shown in Fig. 7. In this case, the charge transport is enabled via the long distance coherent tunneling mechanism, which means that the localized electron of the left dot can be transferred to the right dot via an effective hopping strength mediated by the central dot.[25] When we consider U_{LR} or tune $t_{\ell,j}$ away from $3\Gamma_0$ (not shown here), the maximum PF for SCTQD would occur at the orbital-depletion condition.

4 Summary

To reveal the QI and orbital filling effects on charge/heat transport in QDSL and molecule junctions, we have theoretically investigated the TE coefficients of TQDM with a full many-body solution. Our theoretical work can serve as a guideline for the design of nanoscale TE devices. The destructive QI of G_e is found to be very robust with respect to temperature variation. This implies that it is possible to achieve the destructive QI of G_e at high temperatures. Furthermore, the Seebeck coefficient can be made large with a vanishingly small electrical conductance when temperature increases. From the results of various QDMs with a few electrons, we have

demonstrated that the measurement of Seebeck coefficient, S is a powerful tool to reveal the many-body effect of nanostructures, since S is influenced much more than G_e. To achieve maximum power factor in the case of TQDM prefers the orbital-filling situation (with N=6). However, for SCTQD in general it is preferable to the orbital-depletion situation with ($N \leq 1$) and likely for serially coupled QDMs with more dots. It is desirable to compare current results including all Green functions and electron correlations with those calculated by the Hartree-Fock approximation (HFA)[22–24] to examine the validity of mean-field approach. Such a comparison for SCTQD has been carried out.[35] It is found that HFA works well only for the orbital-depletion situation and high temperatures.

5 Acknowledgments

References

1 A. J. Minnich, M. S. Dresselhaus, Z. F. Ren and G. Chen, *Energy Environ. Sci.*, 2009, **2**, 466–479.
2 M. Zebarjadi, K. Esfarjani, M. S. Dresselhaus, Z. F. Ren and G. Chen, *Energy Environ. Sci.*, 2012, **5**, 5147–5162.
3 G. Mahan, B. Sales and J. Sharp, *Physics Today*, 2008, **50**, 42–47.
4 R. Venkatasubramanian, E. Siivola, T. Colpitts and B. O'quinn, *Nature*, 2001, **413**, 597–602.
5 A. I. Boukai, Y. Bunimovich, J. Tahir-Kheli, J.-K. Yu, W. A. Goddard Iii and J. R. Heath, *Nature*, 2008, **451**, 168–171.
6 T. C. Harman, P. J. Taylor, M. P. Walsh and B. E. LaForge, *Science*, 2002, **297**, 2229–2232.
7 K. F. Hsu, S. Loo, F. Guo, W. Chen, J. S. Dyck, C. Uher, T. Hogan, E. K. Polychroniadis and M. G. Kanatzidis, *Science*, 2004, **303**, 818–821.
8 M. Dresselhaus, G. Chen, M. Tang, R. Yang, H. Lee, D. Wang, Z. Ren, J.-P. Fleurial and P. Gogna, *Advanced Materials*, 2007, **19**, 1043–1053.
9 D. M.-T. Kuo and Y.-C. Chang, *Nanotechnology*, 2013, **24**, 175403.
10 P. Murphy, S. Mukerjee and J. Moore, *Phys. Rev. B*, 2008, **78**, 161406.
11 D. M.-T. Kuo and Y.-C. Chang, *Phys. Rev. B*, 2010, **81**, 205321.
12 J. Liu, Q.-f. Sun and X. C. Xie, *Phys. Rev. B*, 2010, **81**, 245323.
13 M. Wierzbicki and R. Swirkowicz, *Phys. Rev. B*, 2011, **84**, 075410.
14 D. Sánchez and L. m. c. Serra, *Phys. Rev. B*, 2011, **84**, 201307.
15 P. Trocha and J. Barnaś, *Phys. Rev. B*, 2012, **85**, 085408.
16 G. Chen and C. Tien, *Journal of Thermophysics and Heat Transfer*, 1993, **7**, 311–318.
17 G. Chen, *Journal of Heat Transfer*, 1997, **119**, 220–229.

18 D. Li, Y. Wu, P. Kim, L. Shi, P. Yang and A. Majumdar, *Applied Physics Letters*, 2003, **83**, 2934–2936.

19 A. I. Hochbaum, R. Chen, R. D. Delgado, W. Liang, E. C. Garnett, M. Najarian, A. Majumdar and P. Yang, *Nature*, 2008, **451**, 163–167.

20 R. Chen, A. I. Hochbaum, P. Murphy, J. Moore, P. Yang and A. Majumdar, *Phys. Rev. Lett.*, 2008, **101**, 105501.

21 D. L. Nika, E. P. Pokatilov, A. A. Balandin, V. M. Fomin, A. Rastelli and O. G. Schmidt, *Phys. Rev. B*, 2011, **84**, 165415.

22 J. P. Bergfield and C. A. Stafford, *Phys. Rev. B*, 2009, **79**, 245125.

23 J. P. Bergfield and C. A. Stafford, *Nano Letters*, 2009, **9**, 3072–3076.

24 J. P. Bergfield, M. A. Solis and C. A. Stafford, *ACS Nano*, 2010, **4**, 5314–5320.

25 C.-C. Chen, Y.-c. Chang and D. M. T. Kuo, *Phys. Chem. Chem. Phys.*, 2015, **17**, 6606–6611.

26 H. Haug, A.-P. Jauho and M. Cardona, *Quantum kinetics in transport and optics of semiconductors*, Springer, 2008.

27 A.-P. Jauho, N. S. Wingreen and Y. Meir, *Phys. Rev. B*, 1994, **50**, 5528–5544.

28 A. Oguri, S. Amaha, Y. Nishikawa, T. Numata, M. Shimamoto, A. C. Hewson and S. Tarucha, *Phys. Rev. B*, 2011, **83**, 205304.

29 M. Busl, G. Granger, L. Gaudreau, R. Sánchez, A. Kam, M. Pioro-Ladriere, S. Studenikin, P. Zawadzki, Z. Wasilewski, A. Sachrajda and G. Platero, *Nature nanotechnology*, 2013, **8**, 261–265.

30 F. R. Braakman, P. Barthelemy, C. Reichl, W. Wegscheider and L. M. Vandersypen, *Nature nanotechnology*, 2013, **8**, 432–437.

31 S. Amaha, W. Izumida, T. Hatano, S. Teraoka, S. Tarucha, J. A. Gupta and D. G. Austing, *Phys. Rev. Lett.*, 2013, **110**, 016803.

32 R. Sánchez, F. Gallego-Marcos and G. Platero, *Phys. Rev. B*, 2014, **89**, 161402.

33 C. M. Guédon, H. Valkenier, T. Markussen, K. S. Thygesen, J. C. Hummelen and S. J. van der Molen, *Nature Nanotechnology*, 2012, **7**, 305–309.

34 C. W. J. Beenakker and A. A. M. Staring, *Phys. Rev. B*, 1992, **46**, 9667–9676.

35 Y.-C. Tseng, D. M.-T. Kuo, Y.-C. Chang and C.-W. Tsai, *arXiv preprint arXiv:1504.06082*, 2015.

Physical Chemistry Chemical Physics Accepted Manuscript